Evolution of the electronic structure of $La_{2-x}Sr_xCuO_4$ with doping determined by positron-annihilation spectroscopy

R. H. Howell
Lawrence Livermore National Laboratory, P.O. Box 808, Livermore, California 94550

P. A. Sterne
Lawrence Livermore National Laboratory, P.O. Box 808, Livermore, California 94550 and University of California, Davis, California 94550

M. J. Fluss
Lawrence Livermore National Laboratory, P.O. Box 808, Livermore, California 94550

J. H. Kaiser
Physics Department, University of Texas, Arlington, Texas 76019

K. Kitazawa
Department of Industrial Chemistry, University of Tokyo, Tokyo, Japan

H. Kojima
Physics Department, Yamanashi University, Kofu, Japan
(Received 21 October 1993)

We have measured and calculated the electron-positron momentum distribution of $La_{2-x}Sr_xCuO_4$ samples for Sr concentrations of 0, 0.1, 0.13, and 0.2. Measured distributions were obtained at room temperature with high statistical precision, greater than 4×10^8 events, in the Lawrence Livermore National Laboratory positron-annihilation angular correlation spectrometer on single-crystal samples fabricated using the traveling solvent floating zone technique. Corresponding theoretical momentum-density calculations were performed using the linear muffin-tin-orbital method. The momentum distribution of all samples contained features derived from the overlap of the positron distribution with the valence electrons. In addition, discontinuities typical of a Fermi surface are seen in the doped samples. The form and position of these features are in general agreement with the Fermi surface and overall momentum distributions as predicted by band theory. However, the evolution of the Fermi surface with doping differed significantly from expectations based on single electron band theories.

INTRODUCTION

The electronic structure of the high-temperature cuprates and its relationship to the charge carrier doping is central to the discussion of many theories of high-temperature superconductivity. The observation of a Fermi edge and the determination of the shape and position of the Fermi surface for systems having different levels of hole doping can provide a stringent test for electronic structure calculations and superconducting theories. The existence of the Fermi surface for multiple bands has been demonstrated in the high-temperature superconductors by photoemission,[1,2] de Haas–van Alphen,[3] and positron annihilation[4–6] for perovskite systems containing multiple copper-oxygen planes and copper-oxygen chains. These studies were conducted with the best quality, fully optimized superconducting samples. The positions of the observed Fermi surfaces were found to be in remarkable agreement with band theory.[7–9]

Up until now there has been only one similar measurement on the less complicated perovskite superconductors containing only one copper-oxygen plane in their structure. The Fermi surface of the *n*-type $Nd_{2-x}Ce_xCuO_{4-\delta}$ has been mapped in angle-resolved photoemission and found to be similar to band-theory predictions for samples with 0.15 and 0.22 Ce concentrations.[10] To our knowledge there have been no previous studies of the Fermi surface in hole-doped systems such as $La_{2-x}Sr_xCuO_4$. Data for such systems are especially important as many theories containing effects of highly correlated electrons are based on conduction in a single copper-oxygen plane. In positron-annihilation measurements, an additional advantage is obtained by the strong overlap of the positron wave function with the copper-oxygen planes in this system.[11] This is in contrast to the positron distribution in other systems where the positron wave function overlaps strongly with other features in the structure such as the copper-oxygen chains in $YBa_2Cu_3O_7$.[4]

There have been limited observations on the effects that hole doping on the copper-oxygen planes will have on the Fermi surface. Variations in the photoelectron spectra near the Fermi-surface crossing have been observed in photoemission for $YBa_2Cu_3O_7$ for several oxygen concentrations in the copper-oxygen chains.[6]

0163-1829/94/49(18)/13127(10)/$06.00

We present a detailed examination of the Fermi surface in $La_{2-x}Sr_xCuO_4$ and its sensitivity to Sr concentration. Electronic distributions were measured by two-dimensional angular correlation of annihilation radiation of electrons and positrons (ACAR). These data provide an electron occupancy distribution weighted by the positron sampling function in momentum space. Varying the Sr concentration in the La lattice is expected to directly change the carrier concentration in the adjacent copper-oxygen planes and produces changes in the electron occupancy that are easily seen by ACAR in this system. Measurements have been made for Sr concentrations of 0.0, 0.1, 0.13, and 0.2 to span the range from insulating behavior to over doping for maximum transition temperature. These data have been compared in detail with corresponding band-theory calculations for reference of features due to positron wave-function sampling and band filling.

MEASUREMENTS

The electron-positron momentum distribution was measured using a state of the art angular correlation spectrometer at Lawrence Livermore National Laboratory. The spectrometer is constructed from two Anger camera, position sensitive gamma-ray detectors separated by 26 m and a source-sample chamber located midway between them. Each detector consists of a 500 mm diameter by 10 mm thick NaI(Tl) scintillator backed by an array of photodetectors. The location of a 511 keV gamma-ray interaction can be determined to within 3 mm and the angle between two gamma rays can be determined to within 0.4 mrad. Relative angles for correlated events were calculated and stored in a matrix having 0.16×0.16 mrad^2 dispersion.

Single-crystalline samples of $La_{2-x}Sr_xCuO_4$ material were suspended on two Tungsten 50 micron wires attached to a ring goniometer so that positron interactions with the sample holder are minimized. Sample holder contributions are estimated at less than 2% of the total measured distribution. Small contributions of a few percent were observed for sample orientations exposing the epoxy fixing the samples to the wires to the positron flux. Samples were oriented off line by Laue photography so that the c axis of the sample would be coincident with the detector-detector axis and then transferred to the source-sample chamber. Data were collected at room temperature in spectra of about 2×10^7 counts which were individually examined for consistency and then combined into a total distribution having between 4×10^8 and 5×10^8 counts total for each sample. Angular data were corrected by an angular-dependent detector system efficiency calculated from the uncorrelated results of each detector. After detailed inspection of these data they were folded to take advantage of the crystalline symmetry.

Samples used in this experiment were fabricated using the traveling solvent floating zone technique. Several samples were cut from each crystal boule and measurements of transport and other characteristics were carried out on several samples fabricated by this method.[12–14] The insulating, $x=0.0$, sample was annealed in an argon atmosphere at 800 °C for 100 h to remove the oxygen-rich superconducting phase, after which it had an antiferromagnetic transition at 305 K. Those samples with Sr doping at 0.1, 0.13, and 0.2 had sharp superconducting transitions at 26 K, 33 K, and 26 K, respectively, and metallic resistivity in the normal state.[12]

CALCULATIONS

Complementary calculations of the electron-positron momentum density were performed using the linear muffin-tin orbital (LMTO) method and the local density approximation (LDA) for the electron-electron and electron-positron interactions.[15] The experimental momentum densities for these systems show strong variations associated with the overlap of electron and positron wave functions in the unit cell, and these strong effects must be accounted for before the weaker Fermi-surface-related features can be identified. The electronic structure calculations play two important roles in analyzing the experimental data. First, they provide a description of the dominant wave-function effects and permit us to distinguish between possible Fermi-surface features and wave-function effects. Second, they provide a prediction of the expected variation of Fermi-surface features with doping in the simplest realistic theory which contains both electron-positron wave-function effects and a Fermi surface, namely LDA band theory.

Electron and positron wave functions were calculated from potentials produced by self-consistent LMTO electronic structure calculations. The electron-positron momentum density, $\rho(\mathbf{p})$, is calculated in the independent particle model in which

$$\rho(\mathbf{p})=\rho(\mathbf{k}+\mathbf{G})=\sum_{n,\mathbf{k}\text{occ}}\left|\int d^3\mathbf{r}\,\psi^{\text{el}}_{n,\mathbf{k}}(\mathbf{r})\psi^{\text{pos}}(\mathbf{r})e^{-i\mathbf{p}\cdot\mathbf{r}}\right|^2, \quad (1)$$

where ψ^{el} is the electron wave function, ψ^{pos} is the positron wave function, $\mathbf{G}$ is a reciprocal lattice vector, and the sum extends over all occupied electron states. The electron wave functions are calculated on a grid covering one eighth of the orthorhombic zone, the positron wave function is calculated at $\mathbf{k}=0$, and these are used to calculate the electron-positron momentum density throughout momentum space. Using symmetry, the momentum density is calculated in just one octant of reciprocal space. Integration along the c axis is then performed to give the theoretical two-dimensional ACAR spectrum corresponding to the experimental crystal orientation.

Since the LDA predicts metallic behavior for the undoped antiferromagnetic insulator, the calculations were modified by the methods of Ref. 16 for the undoped samples. Sr doping was approximated by either rigid band shifts on the insulating band structure or by explicit supercell calculations at 0.25 Sr concentration. Calculations were also done for both orthorhombic distortion and undistorted lattices by specifically including the displacement of the oxygen atoms in the orthorhombic case.

Positron annihilation occurs with all electrons in the system resulting in a highly isotropic distribution with

small deviations brought about from the distribution of the positron wave function, the core and valence electrons, and the electrons in the conduction band. In oxide materials, contributions from the variations of the electron and positron wave functions can dominate the Fermi-surface contribution from conduction electrons. Fermi-surface structures are characterized by occupation of the electron states only inside boundaries defined by the Fermi surface. Thus the characterizing feature of the Fermi surface is a sharp change in the electron-positron momentum density, but this feature must be observed in the presence of the stronger wave-function-induced variations.

DATA REDUCTION

The experimentally measured momentum density forms a strongly isotropic distribution, so the data must be reduced to enhance the nonisotropic features. There are two commonly used techniques for this enhancement: (a) calculation of the residual anisotropy after subtraction of the isotropic part and (b) calculation of a **k**-space density by reduction of the data into a single, central Brillouin zone by the Lock-Crisp-West (LCW) theorem. Both of these techniques can enhance evidence of the anisotropic parts of the data distribution but each has relative advantages. Also, to facilitate comparison between theory and experiment, it is important to analyze the experimental and theoretical momentum densities in parallel and subject them to the same procedures. The anisotropic residual and LCW data renditions can enhance different features but in general any significant feature in the data or in the corresponding calculations should be discernible in both renditions.

Calculation of the anisotropic residual is an *ad hoc* procedure performed by calculating an isotropic distribution from the average value of the data at each radial momentum and then subtracting this distribution from the total data set. The anisotropic residual displays the data on a full, **p**, momentum scale normally encompassing several crystal zones. This operation requires no *a priori* assumptions about the condition of the sample so that features may be discussed without reference to even the crystal lattice values. In cases where symmetry conditions allow a clear separation of features, such as in the ACAR data for $YBa_2Cu_3O_{7-\delta}$ (YBCO), the Fermi surface can be identified and values of its position determined in the first- and higher-order Brillouin zones without any reference to theory. However, the residual anisotropy has the disadvantage of obscuring radially symmetric features and could even "hide" a spherical Fermi surface. It is also difficult to make a separation of effects from conduction electrons and other features such as those resulting from the positron wave-function distributions in cases where the symmetry of all of these features is the same.

Calculation of the LCW **k**-space density is performed by adding values of the data distribution at momentum values $\mathbf{p}=\mathbf{k}+\mathbf{G}$ corresponding to identical crystal **k** momentum values in the first- and higher-order Brillouin zones. This procedure is only justified for the case of a delocalized positron in a periodic lattice with known periodicity and requires that the crystal phase of the sample be specified. By its nature it enhances the contribution of features having the lattice periodicity, such as the Fermi surface, at the expense of other effects. However, this display of the data is highly condensed and can contain the contributions from backgrounds or defects that are removed in the anisotropic residual. In appropriate cases, we have removed the contribution of epoxy holding the samples to the support wires. No corrections were made for possible defect-related contributions or other backgrounds.

In order to display the data after condensation into the first Brillouin zone by the LCW procedure we must determine the symmetry and lattice constants for the measured structure. The $La_{2-x}Sr_xCuO_4$ system presents a special problem in this regard, as there is a second-order phase transition from one face-centered orthorhombic to body-centered tetragonal as a function of temperature and Sr concentration, with low temperature and low Sr concentration favoring the orthorhombic structure. We have chosen to display all of the data in the orthorhombic unit cell in order to have a consistent comparison for the results of the several Sr dopings. This is possible since the orthorhombic unit cell can always be constructed out of tetragonal unit cells.

DATA

Experimental and theoretical anisotropic residual distributions are shown in Fig. 1 for data taken for a Sr doping of 0.13. The measurements generally reproduce the features determined in a low statistics measurement of La_2CuO_4.[16] The theoretical calculation contains all of the major features of the measured distribution and quantitatively reproduces the momentum at which the dominant high and low positions are found. Even the weaker features found at higher momentum are reproduced in these calculations. However, the crosslike feature centered at the origin in the calculation is not observed in the experimental data. This crosslike feature was seen in data on La_2CuO_4 in Ref. 11 but only in measurements taken at low temperature, so its absence in the present data may be a consequence of room-temperature measurement. The present calculations represent a marked improvement over the qualitative agreement of the atomic orbital–molecular orbital calculations of Ref. 11 which only described the effects from the positron distribution and did not incorporate the full symmetry of the crystalline structure. The fourfold symmetry of the experimental data is a consequence of the body-centered tetragonal symmetry of the 0.13 sample at room temperature. However, since the orthorhombic phase would be expected to be randomly twinned, a smeared fourfold symmetry would also be expected for samples in the orthorhombic phase. The close correspondence between calculated and measured features at even the highest measured momenta suggests that the positron distribution effects are very well described in the calculations.

The calculations contain contributions from both filled valence bands and the conduction-band Fermi surface. Thus by manipulating the calculation we can identify features in the anisotropic distribution that are related to

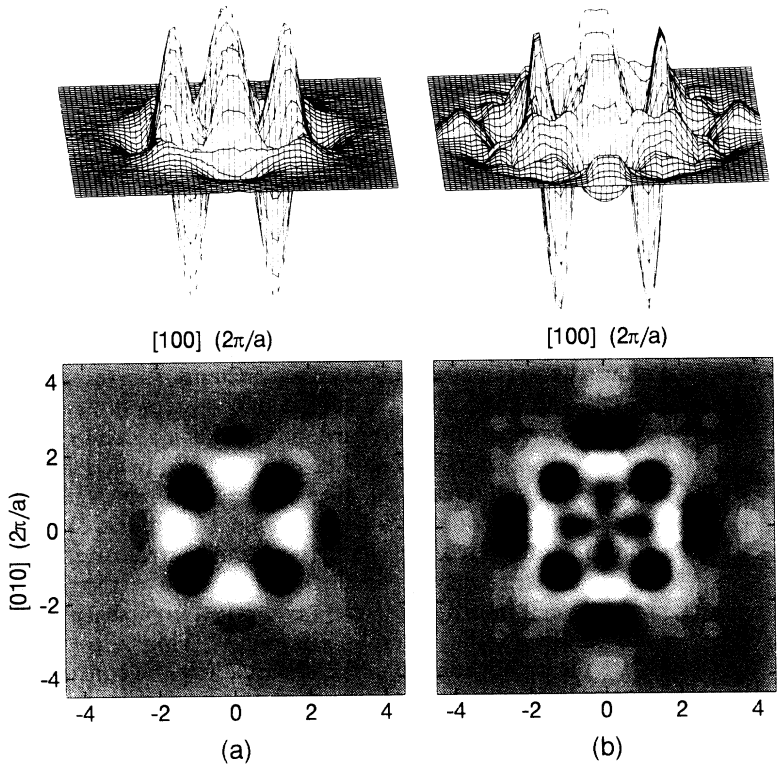

FIG. 1. Residual anisotropy of the experimental (a) electron-positron momentum density of $La_{1.87}Sr_{0.13}CuO_4$ and corresponding calculation (b). Darker shading corresponds to lower values.

the Fermi surface and those related to the positron distribution, or wave-function effects. From this examination we have determined that the major features of the Fermi surface are not strongly reflected in the anisotropic residual. The success of identifying the chain Fermi surface in YBCO (Ref. 4) was only possible due to the twofold symmetry of the Fermi surface compared to the fourfold symmetry of the rest of the unit cell. In $La_{2-x}Sr_xCuO_4$, both the Fermi-surface features and the strong electron-positron wave-function effects have fourfold symmetry, so there is no easy way to separate these two contributions. The calculations clearly demonstrate the Fermi surface may not always be readily apparent in this display of the data.

The LCW-treated experimental data for $x=0.13$ is seen in Fig. 2 along with calculations for $x=0.15$ and an antiferromagnetic insulator. The effects of the positron distribution and valence electrons are evident in the insulating calculation where there is no Fermi surface, and features found in the measured data associated with these effects are reproduced. The depression at the zone-center gamma and the elevation near the zone corners can be seen to be primarily due to wave-function effects. There is another feature in the data in the form of a deep depression at the zone boundary which can be seen in the metallic calculation, but is absent in the insulator calculation. In the calculation, this feature is unambiguously identified as resulting from the Fermi surface. With the aid of the calculated results we can then identify the similar feature in the measurement as resulting from the Fermi surface of the Cu-O planes.

In band models, doping of holes in the Cu-O planes results in an increasingly large unoccupied region in the Brillouin zone, a "hole pocket." The effect of hole doping can be seen in our calculations by shifting the Fermi

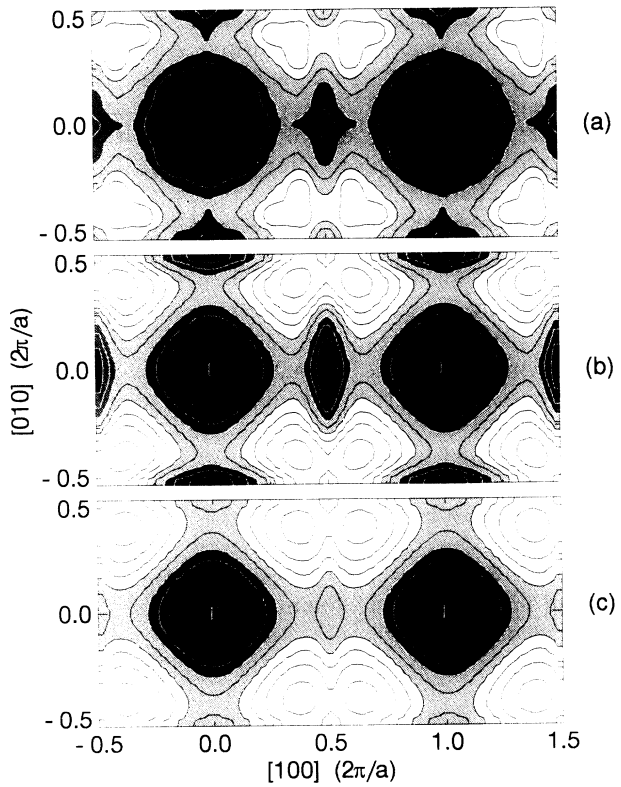

FIG. 2. Electron-positron k-space densities obtained using the Lock-Crisp-West folding procedure into an orthorhombic $La_{2-x}Sr_xCuO_4$ zone. (a) Experimental results for $x=0.13$. (b) Calculations for $x=0.15$ and (c) calculations for an antiferromagnetic insulator. Note the depletion of electron-positron momentum density at (0.5,0.0) in (a) and (b) indicating the presence of a Fermi surface. Darker shading corresponds to lower values.

energy by values of −5, −10, and −15 mRy. These correspond to three separate Sr concentrations very near the experimental sample values as shown in Fig. 3. Since the evolution of features in these calculations is continuous, fine tuning the energy shift to correspond to exact doping levels is unnecessary. The hole pocket on the zone boundary is seen to increase in area and depth as the doping level is increased and the position of the peaks due to the positron distribution effects is moved closer to the zone center for the more highly doped material. These detailed calculations based on an LDA treatment of the electron-electron interactions are not expected to give a reliable description of the electronic structure of the excited-state properties of the system. However, they are qualitatively consistent with the predictions of other band theories, many of which are based on a single copper-oxygen band, which show that the hole doping occurs in the same region of the Brillouin zone as that indicated by LDA calculations.

EFFECTS OF DOPING ON THE FERMI SURFACE

The features in the experimental data varied systematically as doping was changed and there is a strong correspondence in general among the data for the superconducting samples. The strength of the anisotropic residual relative to the full spectrum was constant to within 12%, with the $x=0.1$ doping having the least anisotropic residual and $x=0.2$ the most. This suggests that defect contributions are fairly independent of doping, since defects tend to give predominantly isotropic contributions to the momentum density. The shape of the anisotropic part of the distribution and the details of the LCW data are also very similar for the superconducting samples, except for small, systematic variations. Such consistency is strong circumstantial evidence that the details of the positron observations are related to the physics controlled by the Sr content rather than individual sample variations. However, there are distinct differences between the closely corresponding data found for the superconducting samples and that found for the insulating sample. For the insulator, the overall shape of the spectrum was narrower and the relative strength of the anisotropic residual was about one half that of the typical strength for a superconducting specimen. Such variation could be the result of defects introduced into the specimen during the reduction annealing step or result from the positron responding to substantial differences in the insulating unit cell. Whatever its origin, this difference leads to a strong distortion of the LCW of the insulating data, but the anisotropic residual distribution is still very similar in shape to those found in the superconducting samples.

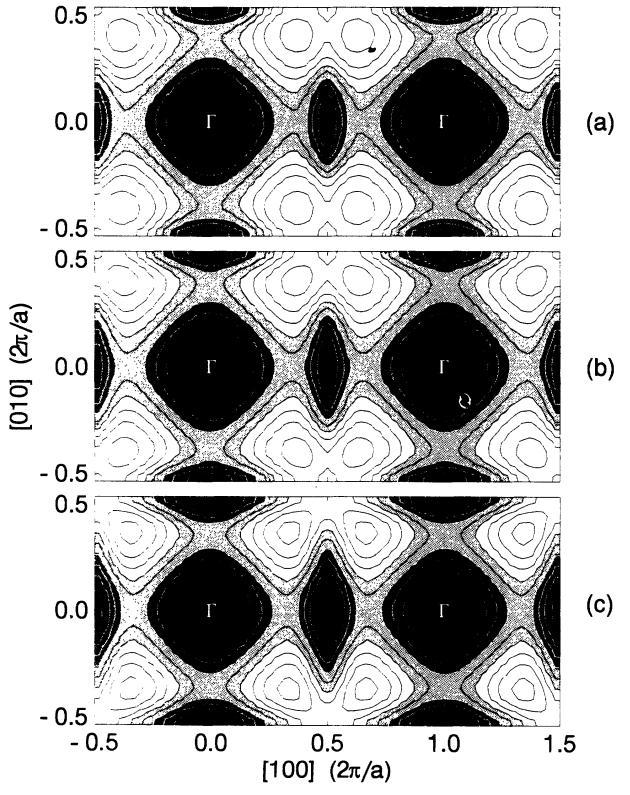

FIG. 3. Theoretical electron-position k-space densities obtained for various dopings obtained by performing the LCW folding procedure into an orthorhombic $La_{2-x}Sr_xCuO_4$ zone for (a) $x=0.11$, (b) $x=0.15$, and (c) $x=0.24$. Darker shading corresponds to lower values.

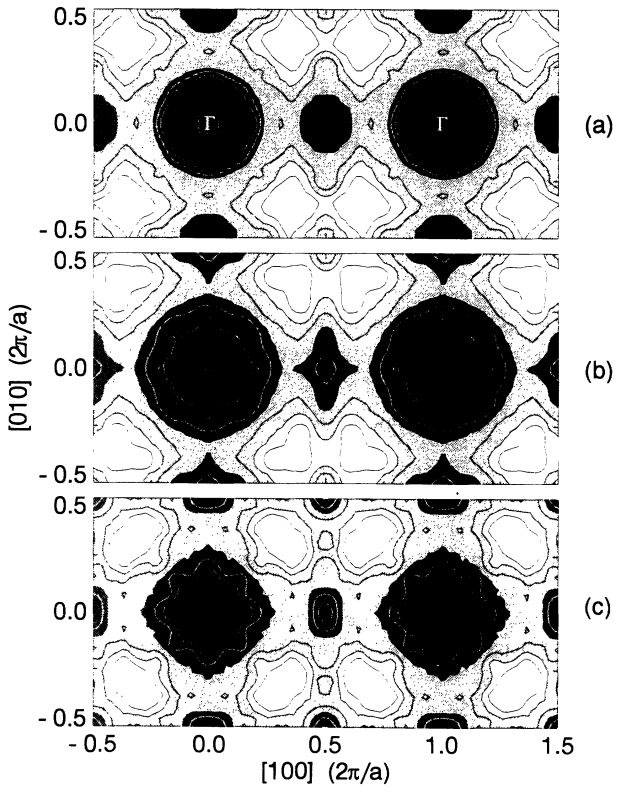

FIG. 4. Experimental electron-positron k-space densities obtained for various dopings obtained by performing the LCW folding procedure into an orthorhombic $La_{2-x}Sr_xCuO_4$ zone for (a) $x=0.1$, (b) $x=0.13$, and (c) $x=0.2$. Darker shading corresponds to lower values.

The LCW display of the data from the superconducting samples (Fig. 4) shows a good overall correspondence in the features of each of the doped samples. The depression at the zone center and the elevated intensity at the zone corners are seen in all of the distributions. The low at the zone edge corresponding to the Fermi-surface "hole pocket" is also easily observed in all three.

Only some of the experimental features have the calculated dependence on doping. The position of the elevated region at the zone edge is closer to the zone center for higher Sr content just as in the calculated distributions and the depth of the well at the zone edge corresponding to the "hole pocket" becomes deeper. These effects are completely consistent with the idea that the number of electrons in a band crossing the Fermi energy decreases with Sr doping and that the effects of doping are consistent with increased hole doping in a band model. However, the area of the hole pocket enclosed by the Fermi surface does not appear to grow larger at higher doping levels. Rather it actually appears to shrink and become less sharply defined as the doping is increased. This is not predicted in a simple band picture such as represented by our calculations in which the Fermi edge becomes more sharply defined and the area of the hole pocket grows larger with increased doping. Nevertheless, the other features seen in the data, such as the shift of the peak at the zone corner and the deepening of the feature at the zone edge, suggest that the general filling of the Brillouin zone is consistent with a band picture. Consequently we interpret this contrary trend in the boundary of the hole pocket area as an apparent smearing of the Fermi surface. This suggests that the change in spectral weight is not localized to a narrow region at the Fermi surface but is spread over a broad range of momenta about the expected Fermi surface position.

CAUSES OF FERMI-SURFACE SMEARING

There are several effects that can lead to the distortion or apparent smearing of the Fermi surface. A sharp Fermi surface is the result of periodic electron motion over large distances in the lattice. If there is a disturbance of this condition due to imperfections in the crystalline structure, such as scattering from a defect or disordered distribution of Sr atoms, then there will be a smearing at the Fermi surface. Scattering centers could include disorder on the Sr sublattice, or point defects from oxygen or cation vacancies. A second possible source of distortion of the Fermi surface could come from doping-dependent distortions of the positron distribution leading to preferential sampling of heavily hybridized levels. A third possibility is that electron correlations have distorted the electron distribution which is then accurately measured by the positron experiment.

In order to evaluate the likelihood of the possibilities for Fermi-surface smearing listed above and to confirm the conclusions derived from the analysis of the doping effects obtained in a single Brillouin zone representation we have performed calculations based on several beginning assumptions and compared them with the data in the first Brillouin zone and anisotropic residual representations.

The interpretation of smearing of the Fermi surface or indeed the identification of the Fermi surface is difficult to achieve in comparisons of the anisotropic residuals. As we have noted these are *ad hoc* procedures and do not enhance any particular set of physical features in the data. On the other hand, if features such as the Fermi surface can be identified, then systematic variations such as smearing must be evident in this display of the data as well. A great difficulty in analyzing the anisotropic residual is the strong contribution of the positron sampling distribution. Essentially all of the features seen in Fig. 1 are due to the positron sampling wave-function effects.

In a further refinement we have subtracted the anisotropic residual for the insulating, $x=0$, sample from the other anisotropic residual distributions after normalization to the residual strength to produce a normalized anisotropic residual. This results in a set of distributions that have the major effects of positron distribution, background, and sample defect contributions minimized in comparison to those effects due to the doping-induced change in occupancy of the conduction electrons. As in our other comparisons we have performed the same operations on the calculated electron-positron momentum densities so that the calculation and data are directly comparable. These distributions for the experiment and corresponding calculations are seen in Figs. 5–7. Figure 5 contains the experimental data compared with calculations performed with a rigid band shift. Figure 6 contains linear displays of the analyzed experimental data of Fig. 5 and Fig. 7 contains the results of several calculations based on differing assumptions.

In the distributions seen in Fig. 5 there is a general correspondence in the large features, i.e., peaks and valleys, of the measured and calculated data. We can see from a comparison of frames (a) and (d) of Fig. 7 that this general agreement was achieved by explicitly including the oxygen displacement in the insulating calculation and excluding that displacement in the doped calculations. This indicates that the momentum density measurement is sensitive to the changes associated with oxygen displacement in the orthorhombic structure and may be observable in the temperature dependence. Other potentially important effects such as explicit wave-function effects introduced by the Sr atom, are seen to be minor in comparison to the oxygen distortion in this regard.

From the calculations in Figs. 5 and 7 we can identify the positions of strong contributions from the Fermi edge in this highly analyzed data display. In general, sharp features typical of a Fermi edge are evident in the experimental data at the positions predicted in the calculations, particularly at the boundaries of the first and third Brillouin zones. To see these clearly in the data, the normalized anisotropic residual distributions have been summed into a set of linear distributions for slices through the momentum space bounded by the Brillouin zone boundaries. Sharp features are visible at expected locations identified by the dotted lines in Fig. 6 in the central- and higher-order Brillouin zones. These features are more sharply defined in the sample with the lowest doping and least sharply defined in the most highly doped sample.

This is completely consistent with our previous interpretation of smearing of the Fermi surface.

Disorder on the sublattice of metallic alloys can often smear the Fermi surface through the strong coupling of shape of the electron bands to the concentration of the alloy constituents. If such an effect were expected in $La_{2-x}Sr_xCuO_4$ then disorder on the Sr sites would be a strong candidate for the observed smearing. However, the shape of the bands changes weakly with Sr content and changes in the band shape from this source cannot account for the observed changes. Minimal differences were observed between rigid shifts of the Fermi energy to accommodate the effects of Sr doping and explicit calculations for Sr 0.25 and 0.5 done in a supercell format. A comparison of the results of rigid band, frames (a) and (e), and supercell calculations, frames (b) and (f), can be made for both normalized residual anisotropies and first Brillouin zone representations in Fig. 7. It is expected that disorder on the La/Sr sublattice should have a minimal broadening effect on the Cu-O plane related Fermi surface since the electrons have only a small overlap with the small potential difference between the La and Sr sites. This is confirmed both by the present supercell calculations and by coherent potential approximation calculations for a disordered La/Sr sublattice which validate the use of the rigid band model in this system.[17,18]

A second potential source of order-disorder scattering that could lead to Fermi-surface smearing is the displacement of the oxygen when in the orthorhombic phase. These distortions may exist as fluctuations even in samples in an overall tetragonal phase[19] and as we have seen can affect the features associated with the distribution of the positron. We have not attempted to quantify the effect of oxygen distortion over all possible ranges. However, a comparison of calculated results with typical distortions shows negligible effects in the position of the Fermi surface but distinct effects on the distribution of the positron wave function. Thus neither Sr disorder nor O distortions seem likely to be the source of the apparent Fermi-surface broadening.

Oxygen and other defects, if present in sufficiently large numbers, can serve as scattering sites which limit the periodicity of the crystal and lead to Fermi-surface smearing. There are no direct determinations of the de-

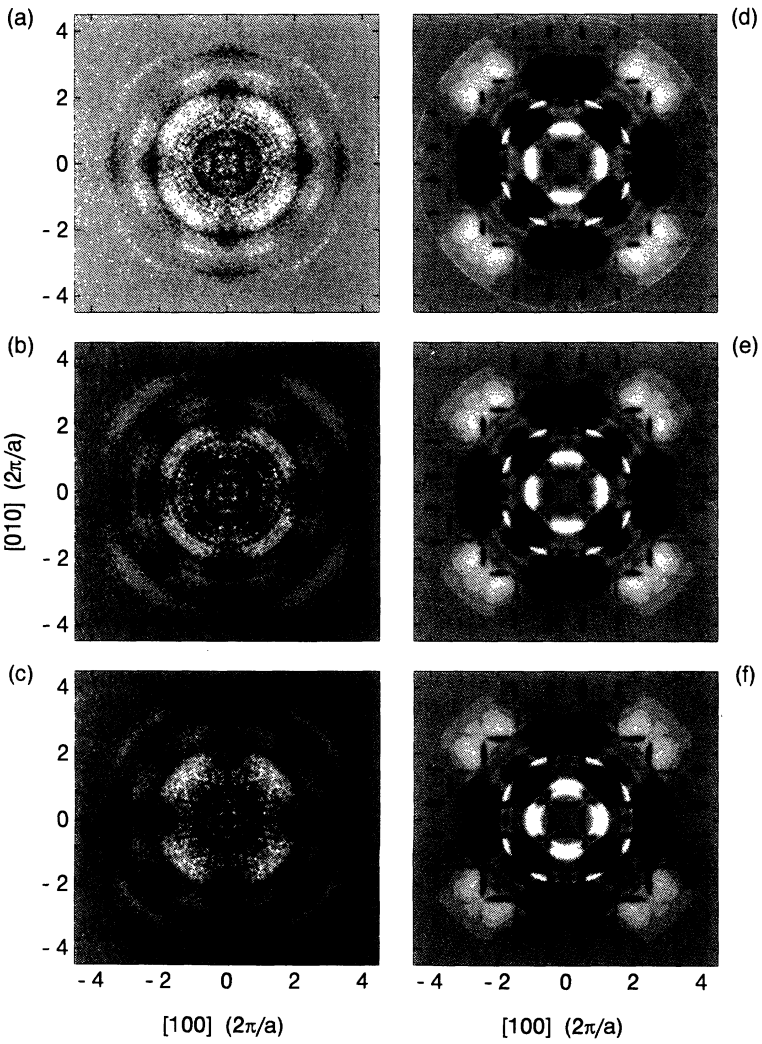

FIG. 5. Normalized anisotropic residuals obtained by subtracting the anisotropic residual calculated for $x=0$ with the oxygen atoms in their distorted orthorhombic positions from the other dopings calculated with the oxygen atoms at their tetragonal sites. This procedure minimizes the contribution of the positron wave-function distribution in the display of the data. Frames (a)–(c) are from the measurements for $x=0.1$, 0.13, and 0.2, respectively, and frames (d)–(g) are for the calculations performed at $x=0.11$, 0.15, and 0.24, respectively.

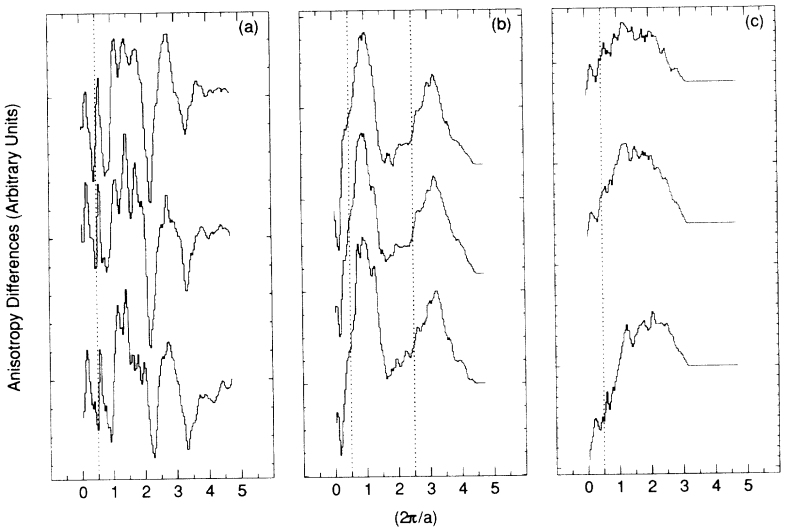

FIG. 6. Measured normalized anisotropic residuals summed between −0.5 and +0.5, frame (a), 1.5 and 2.5, frame (b), and 3.5 to 4.5, frame (c), orthorhombic zone dimensions. For each frame the data are in order of increased doping from top to bottom. Locations where sharp features from the Fermi surface are expected to be strongest are indicated by the dotted lines.

fect densities in these samples. Positron lifetimes were not measured due to the small sample sizes. However, measurements performed on ceramic $La_{2-x}Sr_xCuO_4$ indicate that there is no significant trapping of positrons by defects for the doping levels studied here and the close consistency of the strength of the anisotropic residual for the three doped samples argues that the defect concentration is low for the three dopings and lowest for the $x=0.2$. Since the defect scattering would need to be greatest in the 0.2 in order to explain our results it is unlikely that the increased smearing of the Fermi surface with doping is the result of an increase in the defect

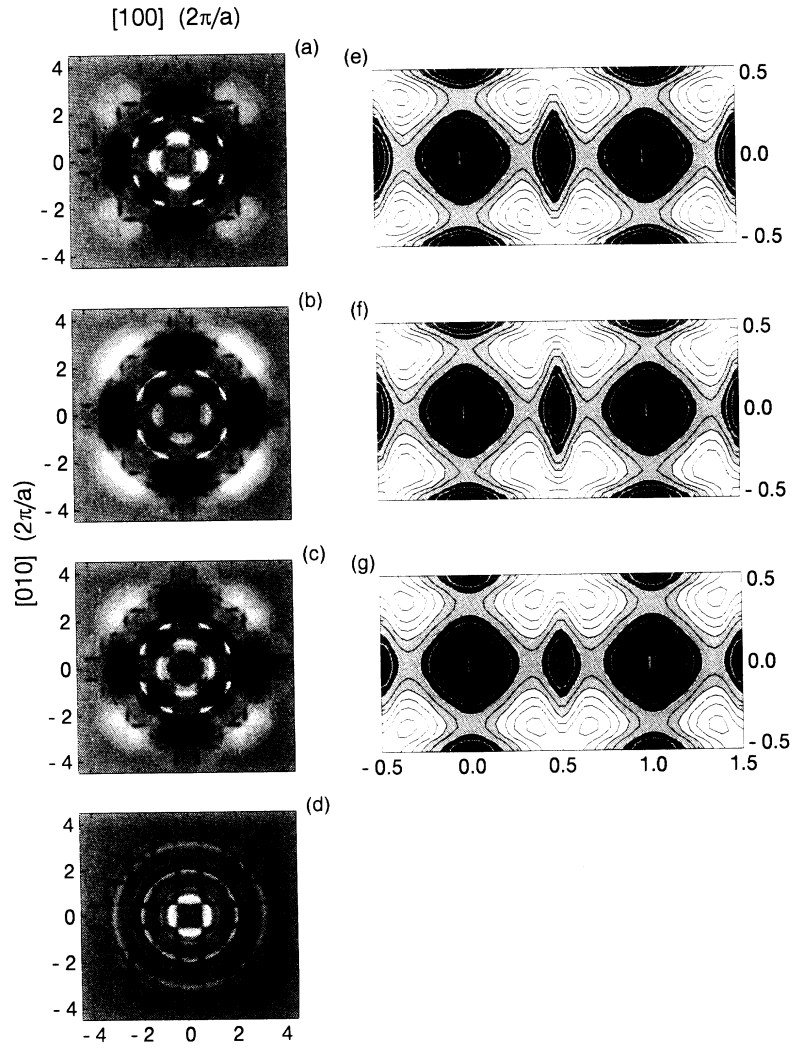

FIG. 7. Calculated normalized residual anisotropies obtained using the same procedure as in Figs. 5(a)–5(d), and k-space densities 5(e)–5(g). Frames (a) and (e) are for $x=0.24$. Frames (b) and (f) are for a supercell containing one Sr atom for each seven La atoms so that $x=0.25$. Frames (c) and (g) are the same as (a) and (e) except that the electron-positron correlation function has been omitted causing a redistribution of the positron away from the Cu-O planes. Frame (d) is the same as (a) except that both the metal and insulator were calculated using the distorted, orthorhombic oxygen positions in the unit cell.

scattering in the $La_{2-x}Sr_xCuO_4$ crystal.

We have tested the likelihood that changes in the positron distribution will result in preferential sampling of a separate part of the electron distribution resulting in a distortion of the Fermi surface. This could occur as the positron becomes repelled from the doped holes in the Cu-O planes. We have explicitly included the Sr in supercell calculations for $x=0.25$ and 0.5 and seen minimal effects as described above. We have also modified the positron distribution by setting the electron-positron correlation potential to zero resulting in a redistribution of the positron wave function as seen in frames (c) and (g) of Fig. 7. Comparison of the anisotropic residual and LCW for these calculations and similar ones having physically appropriate values of the correlation potential showed that details of the positron wave-function effects are changed by redistributing the positron but the shape and position of the Fermi surface and related features are unaffected. Interestingly, the calculated effects due to positron rearrangement were consistent with observed changes in gross features of the experimental momentum density indicating a sensitivity of the positron to doping in this system. However, these changes were not large enough to affect the sharpness of the Fermi breaks in the calculation. Therefore, redistribution of the positron does not appear to be a likely candidate for the observed Fermi-surface variations with Sr doping.

Since these measurements integrate the electron-positron momentum density along the c direction, it is possible that the Fermi surface is not smeared at some position in k space and that the observed result is from a strong distortion of the Fermi surface along the c direction. Since the dispersion along the c axis is included in the calculated results shown for comparison, there would have to be a major deviation between the calculated and physical dispersion in order to explain our data. While this cannot be ruled out experimentally it is unlikely as band calculations, if anything, tend to overemphasize the dispersion in the c direction since the resistivity is insulatorlike in that direction.[14]

Samples containing a distribution of segregated phases might be expected to generate a family of Fermi surfaces, each appropriate to its local Sr concentration. Such a collection of Fermi surfaces would be averaged in an integrated measurement and could lead to an apparent smearing in the Fermi surface. This possibility cannot be excluded by features of the positron data but other characteristics of the samples would also be affected. Such phase segregation would adversely affect the width of the superconducting transition and would also be observable in x-ray and neutron experiments. No indication of phase segregation was found in associated measurements performed on material from the same crystal stock as used in this measurement.

The effects discussed above are all related to potential problems in the sample or in the measurement technique and there is evidence that none of them are strong possibilities for explaining the observed evolution of the Fermi surface and related structures. The only remaining alternative is that the observed evolution is in fact due to changes in the electronic distribution in the sample. There is a large list of correlation effects suggested by other authors that would lead to Fermi-surface smearing with increased doping. In the absence of detailed predictions these data do not differentiate among the possible correlation effects that can describe the basic systematics of our observations except to the extent that increased doping leads to an apparent smearing. This observation also implies that the overdoped material may also have strong correlation effects and would not be expected to behave like a conventional metal. These data do suggest the importance of including correlations in the discussion of the electronic structure of these materials.

CONCLUSIONS

We have measured and calculated the evolution of the electronic structure related to a single copper-oxygen plane in the high-temperature superconductor $La_{2-x}Sr_xCuO_4$. Measurements were done on high-quality single-crystal samples using the angular correlation of positron annihilation to determine the electron-positron momentum density which is closely related to the electron momentum density. Calculations of these same quantities were performed in a first-principles electron-positron band theory. General agreement between the results of these calculations and the data were obtained and the Fermi surface was identified. However, the Fermi surface was smeared as doping increased suggesting that correlation effects or other phenomena are important in the understanding of the electronic structure in these systems.

ACKNOWLEDGMENTS

This work was performed under the auspices of the U.S. Department of Energy by the Lawrence Livermore National Laboratory under Contract No. W-7405-ENG-48. J.H.K. acknowledges financial support from the Robert A. Welch Foundation, Grant No. Y-1135.

[1]C. G. Olson, R. Liu, D. W. Lynch, R. S. List, A. J. Arko, B. W. Veal, Y. C. Chang, P. Z. Jiang, and A. P. Paulias, Phys. Rev. B **42**, 381 (1990).

[2]J. G. Tobin, C. G. Olson, C. Gu, D. W. Lynch, J. Z. Liu, F. R. Solal, M. J. Fluss, R. H. Howell, J. C. O'Brien, H. B. Radousky, and P. A. Sterne, Phys. Rev. B **45**, 5563 (1992).

[3]F. M. Mueller, C. M. Fowler, B. L. Freeman, W. L. Hults, J. C. King, and J. L. Smith, Physica B **172**, 253 (1991).

[4]H. Haghighi, J. H. Kaiser, S. Rayner, R. N. West, J. Z. Liu, R. Shelton, R. H. Howell, F. Solal, and M. J. Fluss, Phys. Rev. Lett. **67**, 382 (1991); H. Haghighi, J. H. Kaiser, S. Rayner, R. N. West, J. Z. Liu, R. Shelton, R. H. Howell, F. Solal, P. A. Sterne, and M. J. Fluss, J. Phys. Chem. Solids **52**, 1535 (1991).

[5]M. Peter, A. A. Manuel, L. Hoffmann, and W. Sadowski, Europhys. Lett. **18**, 313 (1992).

[6]L. C. Smedskjaer, A. Bansil, U. Welp, Y. Fang, and K. G. Bailey, Physica C **192**, 259 (1992).

[7]W. E. Pickett, R. E. Cohen, and H. Krakauer, Phys. Rev. B **42**,

8764 (1990).
[8]J. Yu, S. Massidda, A. J. Freeman, and D. D. Koelling, Phys. Lett. A **122**, 203 (1987).
[9]I. I. Mazin, O. Jepsen, O. K. Andersen, and A. I. Liechtenstein, Phys. Rev. Lett. **68**, 3936 (1992).
[10]D. M. King, Z. X. Shen, D. S. Dessau, B. O. Wells, W. E. Spicer, A. J. Arko, D. S. Marshall, J. DiCarlo, A. G. Loeser, C. H. Park, E. R. Ratner, J. L. Peng, Z. Y. Ki, and R. L. Greene, Phys. Rev. Lett. **70**, 3159 (1993).
[11]P. E. A. Turchi, A. L. Wachs, K. H. Wetzler, J. H. Kaiser, R. N. West, Y. C. Jean, R. H. Howell, and M. J. Fluss, J. Phys. Condens. Matter **2**, 1635 (1990).
[12]S. Kambe, K. Kitazawa, M. Naito, A. Fukuoka, I. Tanaka, and H. Kojima, Physica C **160**, 35 (1989).
[13]S. Kambe, M. Naito, K. Kitazawa, I. Tanaka, and H. Kojima, Physia C **160**, 243 (1989).
[14]T. Kimura, K. Kishio, T. Kobayashi, Y. Nakayama, N. Motohira, K. Kitazawa, and K. Yamafuji, Physica C **192**, 247 (1992).
[15]P. A. Sterne and J. H. Kaiser, Phys. Rev. B **43**, 13 892 (1991).
[16]P. A. Sterne and C. S. Wang, Phys. Rev. B **37**, 7472 (1988).
[17]A. Bansil, S. Kaprzyk, and J. Tobola, *Application of Multiple Scattering Theory to Materials Science,* edited by W. H. Butler, P. H. Dederichs, A. Gonis, and R. Weaver, MRS Symposia Proceedings No. 253 (Materials Research Society, Pittsburgh, 1992), p. 505.
[18]A. Bansil and S. Kaprzyk, Acta Phys. Pol. A **84**, 7 (1993).
[19]T. Egami, W. Domowski, J. D. Jorgensen, D. G. Hinks, D. W. Capone II, C. U. Segre, and K. Zhang, Rev. Solid State Sci. **1**, 247 (1987).

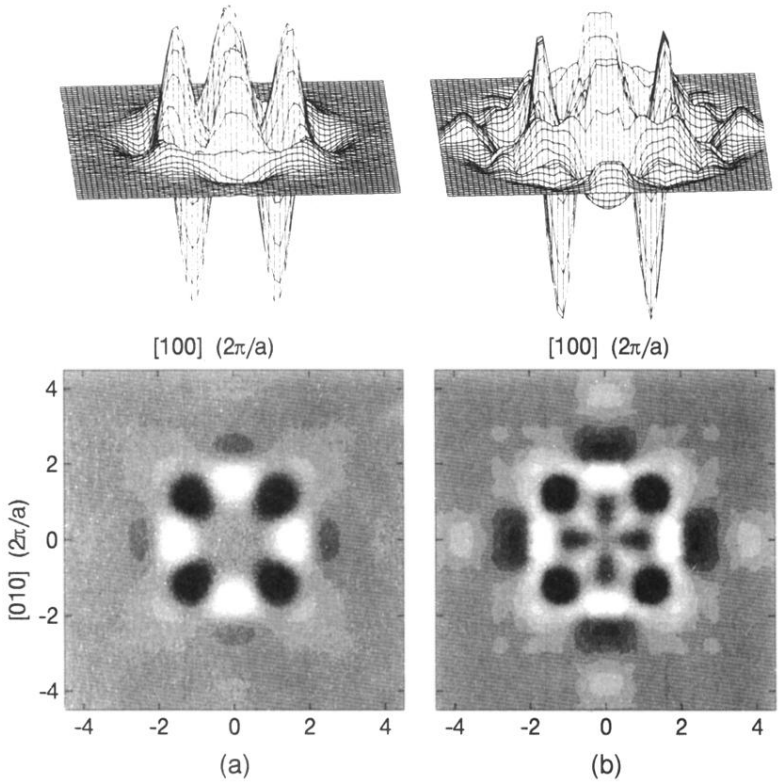

FIG. 1. Residual anisotropy of the experimental (a) electron-positron momentum density of $La_{1.87}Sr_{0.13}CuO_4$ and corresponding calculation (b). Darker shading corresponds to lower values.

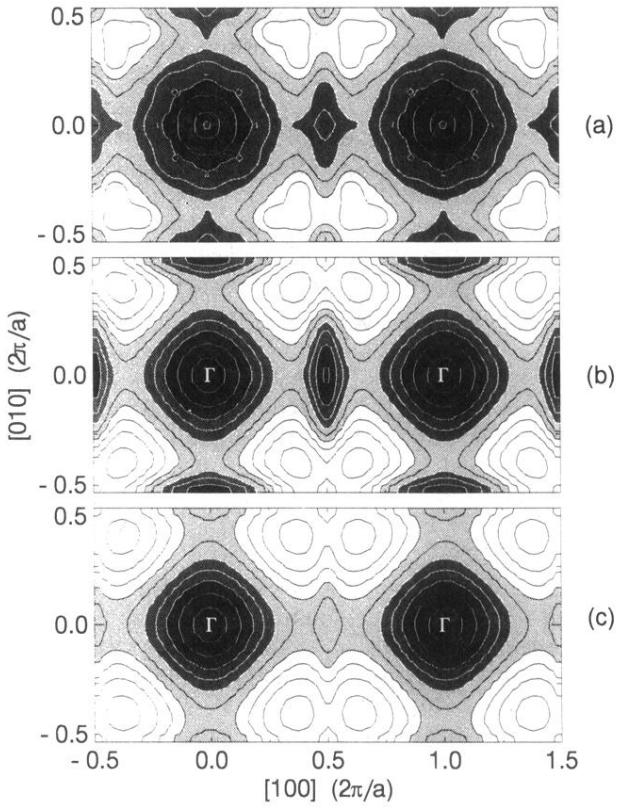

FIG. 2. Electron-positron k-space densities obtained using the Lock-Crisp-West folding procedure into an orthorhombic $La_{2-x}Sr_xCuO_4$ zone. (a) Experimental results for $x=0.13$. (b) Calculations for $x=0.15$ and (c) calculations for an antiferromagnetic insulator. Note the depletion of electron-positron momentum density at (0.5,0.0) in (a) and (b) indicating the presence of a Fermi surface. Darker shading corresponds to lower values.

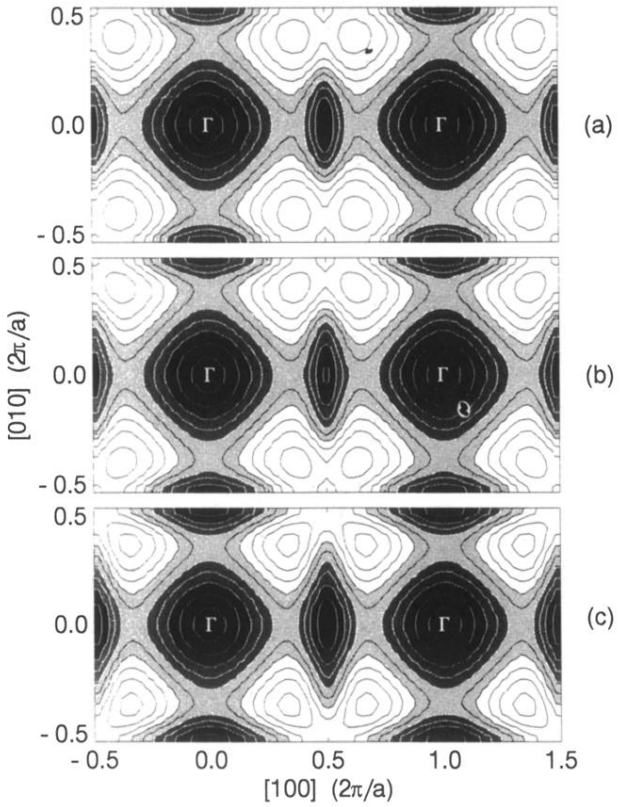

FIG. 3. Theoretical electron-position k-space densities obtained for various dopings obtained by performing the LCW folding procedure into an orthorhombic $La_{2-x}Sr_xCuO_4$ zone for (a) $x=0.11$, (b) $x=0.15$, and (c) $x=0.24$. Darker shading corresponds to lower values.

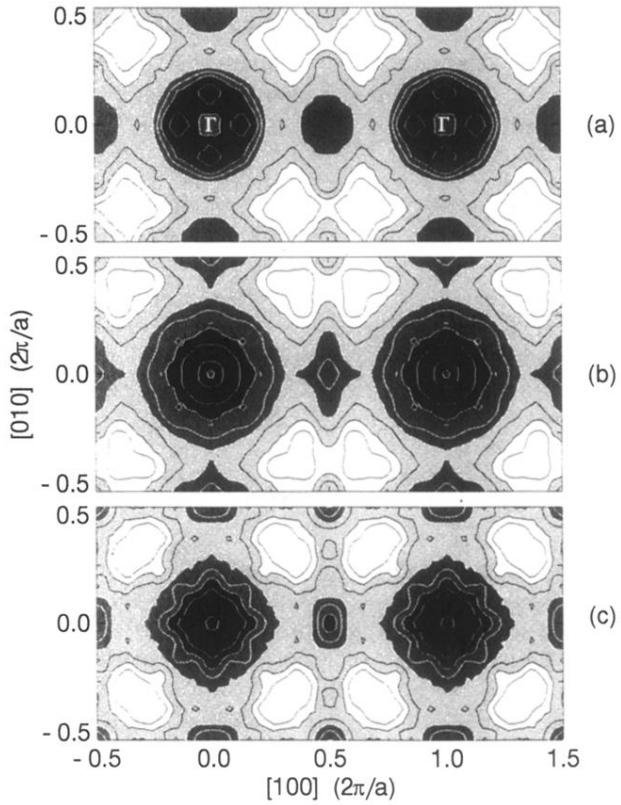

FIG. 4. Experimental electron-positron k-space densities obtained for various dopings obtained by performing the LCW folding procedure into an orthorhombic $La_{2-x}Sr_xCuO_4$ zone for (a) $x=0.1$, (b) $x=0.13$, and (c) $x=0.2$. Darker shading corresponds to lower values.

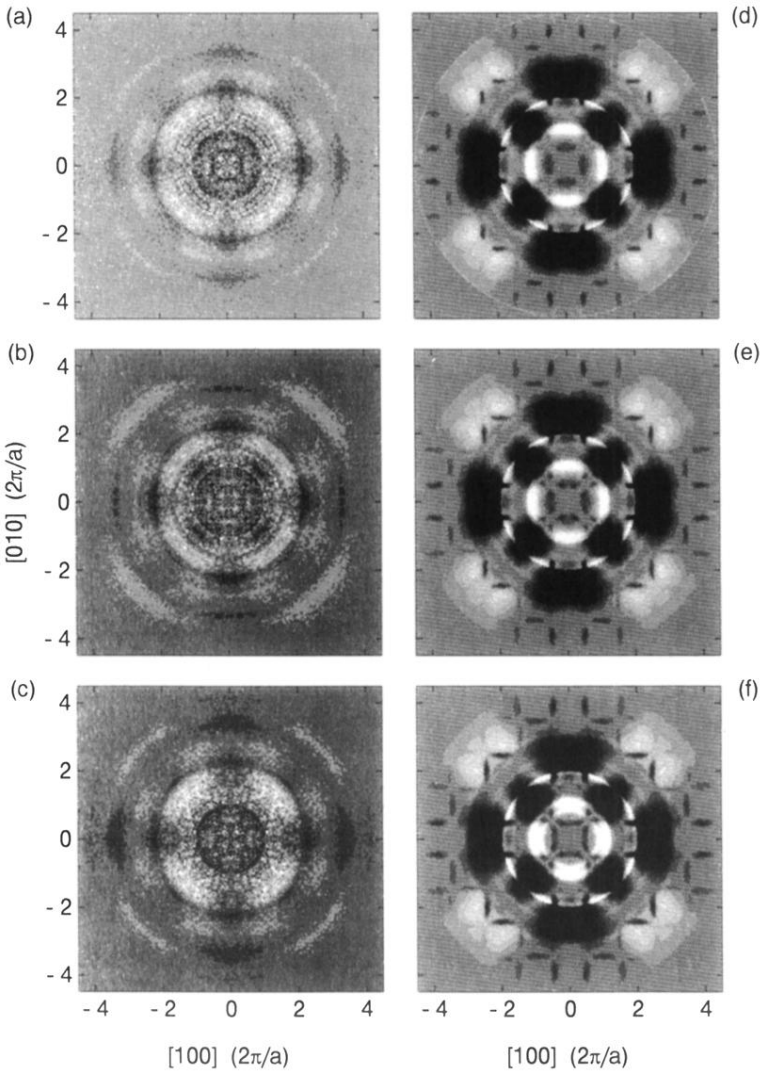

FIG. 5. Normalized anisotropic residuals obtained by subtracting the anisotropic residual calculated for $x=0$ with the oxygen atoms in their distorted orthorhombic positions from the other dopings calculated with the oxygen atoms at their tetragonal sites. This procedure minimizes the contribution of the positron wave-function distribution in the display of the data. Frames (a)–(c) are from the measurements for $x=0.1$, 0.13, and 0.2, respectively, and frames (d)–(g) are for the calculations performed at $x=0.11$, 0.15, and 0.24, respectively.

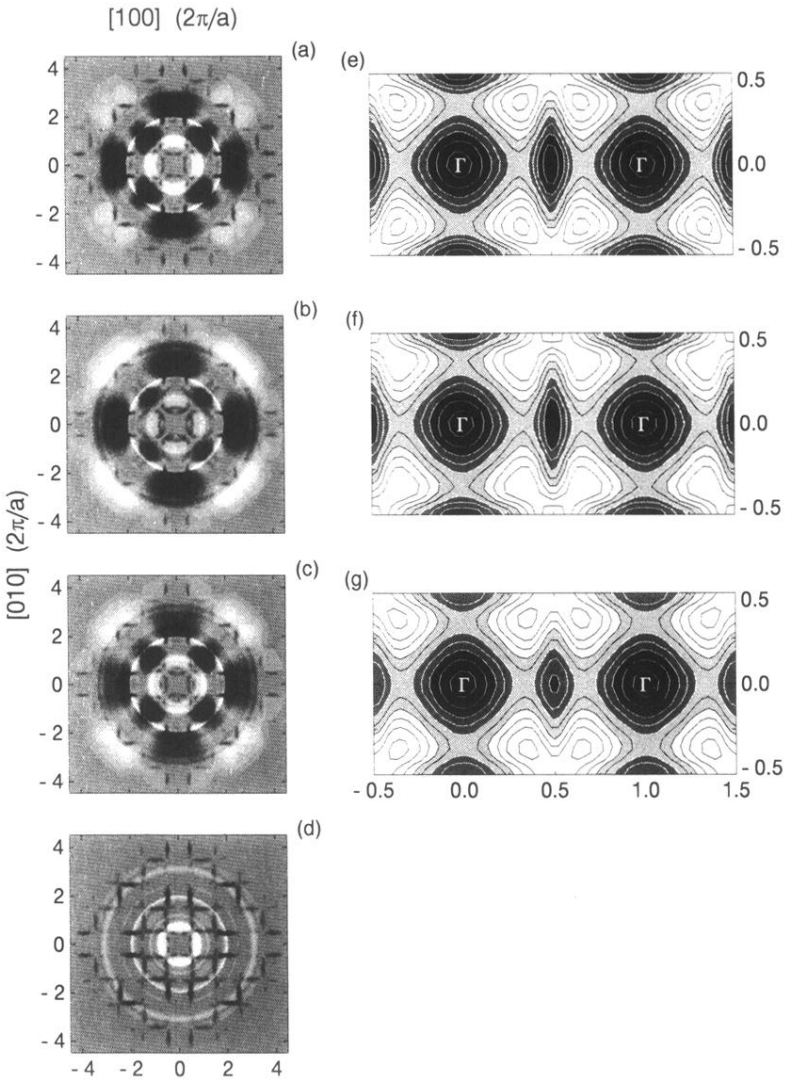

FIG. 7. Calculated normalized residual anisotropies obtained using the same procedure as in Figs. 5(a)–5(d), and k-space densities 5(e)–5(g). Frames (a) and (e) are for $x=0.24$. Frames (b) and (f) are for a supercell containing one Sr atom for each seven La atoms so that $x=0.25$. Frames (c) and (g) are the same as (a) and (e) except that the electron-positron correlation function has been omitted causing a redistribution of the positron away from the Cu-O planes. Frame (d) is the same as (a) except that both the metal and insulator were calculated using the distorted, orthorhombic oxygen positions in the unit cell.